Supporting Information for

An efficient hierarchical self-assembly approach to construct structurally diverse two-step sequential energy-transfer artificial light-harvesting systems

Pei-Pei Jia,[a] Lianrui Hu,[a] Wei-Tao Dou,[a] Xing-Dong Xu,[b] Haitao Sun,[c] Zhi-Yong Peng,[a] Dan-Yang Zhang,[a] Hai-Bo Yang[a] and Lin Xu*[a]*

[a.]Shanghai Key Laboratory of Green Chemistry and Chemical Processes, Shanghai Frontiers Science Center of Molecule Intelligent Syntheses, Wuhu Hospital Affiliated to East China Normal University, School of Chemistry and Molecular Engineering, East China Normal University, Shanghai 200062, P. R. China.

[b.]School of Chemistry and Chemical Engineering, National Engineering Research Center for Colloidal Materials, Shandong University, Jinan, Shandong 250100, P. R. China.

[c.]State Key Laboratory of Precision Spectroscopy, East China Normal University, Shanghai 200062, P. R. China.

Email: lrhu@chem.ecnu.edu.cn; lxu@chem.ecnu.edu.cn

Contents

1. Materials and methods

1.1 General information

All reagents were of analytical purity and used without further treatment. TLC analyses were performed on silica-gel plates, and flash chromatography was conducted using silica-gel column packages. All air-sensitive reactions were carried out under inert N_2 atmosphere. ^{1}H NMR, ^{31}P NMR and ^{13}C NMR spectra were recorded on Bruker 400 MHz Spectrometer (^{1}H: 400 MHz; ^{31}P: 162 MHz; ^{13}C: 100 MHz) or Bruker 500 MHz Spectrometer (^{1}H: 500 MHz; ^{31}P: 202 MHz; ^{13}C: 126 MHz) at 298 K. The ^{1}H NMR chemical shifts are reported relative to residual solvent signals, and ^{31}P NMR resonances are referenced to an internal standard sample of 85% H_3PO_4 (δ 0.0). Coupling constants (J) are denoted in Hz and chemical shifts (δ) are denoted in ppm. 2D NMR spectra (^{1}H-^{1}H COSY and DOSY) were recorded on Bruker 500 MHz Spectrometer (^{1}H: 500 MHz) at 298 K. 2D NOESY was recorded on Bruker 400 MHz Spectrometer (^{1}H: 400 MHz) at 298 K. The HR-ESI mass spectra were performed on Waters (SYNAPTG2-Si) Ion Mobility-Mass Spectrometry.

1.2 UV-Vis absorption, fluorescence emission spectra

UV-vis spectra were recorded in a quartz cell (light path 10 mm) on a Shimadzu UV2700 UV-visible spectrophotometer. Steady-state fluorescence spectra were recorded in a conventional quartz cell (light path 10 mm) on a Shimadzu RF-6000 fluorescence spectrophotometerr (slit width 5 nm/5 nm for ex/em except for special instructions). All spectral measurements were made at room temperature.

1.3 Fluorescence quantum yields

Fluorescence quantum yields were measured in absolutely in solution using a commercial fluorometer with integrating sphere (RF6000, shimadzu).

1.4 Fluorescence lifetimes

The Fluorescence lifetimes were recorded in a quartz cell (light path 10 mm) on the Edinburgh FLS980 transient fluorescence spectrometer.

2. Synthesis and characterization

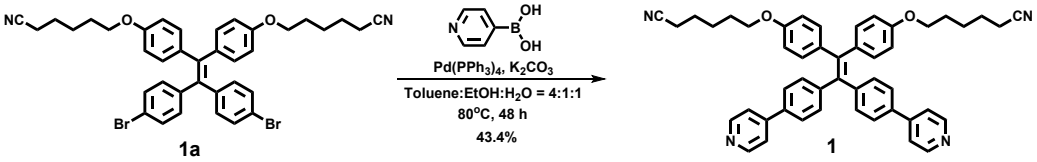

Scheme S1. Synthesis of ligand **1**.

Synthesis of compound **1**: Compound **1a** (1.90 g, 2.67 mmol) and 4-pyridylboronic acid (1.92 g, 16.00 mmol) were added to a 200 mL Schlenk flask and the flask was evacuated and refilled with N_2 three times. Then the freshly distilled toluene (80 mL), ethanol (20 mL), and aqueous K_2CO_3 (2.88 g, 21.36 mmol) solution (20 mL) were added under nitrogen, $Pd(PPh_3)_4$ (601 mg, 0.52 mmol) was then added, and the reaction mixture was stirred at 80°C for 48 h under nitrogen atmosphere. After cooling to room temperature, the product was concentrated and purified by flash column chromatography to afford compound **1** (820 mg, 43.4%) as yellow powder. ^{1}H NMR (500 MHz, acetone-d_6) δ (ppm): 8.59 (d, J = 5.0 Hz, 4H), 7.59 (m, 8H), 7.19 (d, J = 5.0 Hz, 4H), 6.99 (d, J = 10.0 Hz, 4H), 6.71 (d, J = 10.0 Hz, 4H), 3.92 (t, J = 10.0 Hz, 4H), 2.46 (t, J = 5.0 Hz, 4H), 1.72–1.82 (m, 4H), 1.67–1.68 (m, 4H), 1.53–1.62 (m, 4H). ^{13}C NMR (126 MHz, acetone-d_6) δ (ppm): 159.07, 151.35, 147.86, 146.31, 142.96, 138.56, 136.76, 136.34, 133.46, 133.08, 127.18, 121.83, 120.70, 114.70, 68.18, 26.11, 26.07, 17.20. ESI-MS: Calculated for [**1** + H]$^+$: 709.3519; Found: 709.3530.

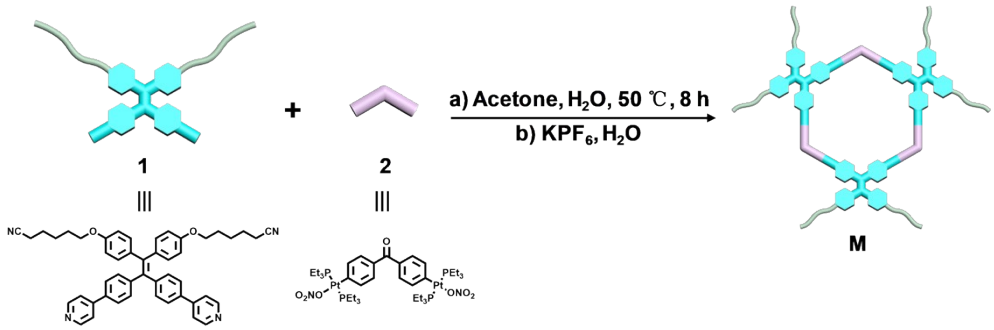

Scheme S2. Synthesis of metallacycle **M**.

Synthesis of metallacycle **M**: The **1** (12.63 mg, 17.82 μmol), and **2** (20.79 mg, 17.82 μmol) were mixed in a 1:1 molar ratio and dissolved in acetone/water (2.4 mL, 5:1,

v/v). The whole reaction mixture was heated at 50℃ for 8 h to yield a homogeneous solution and then cooled to room temperature. Then the addition of a saturated aqueous solution of KPF_6 into the bottle with continuous stirring precipitated the product. The reaction mixture was centrifuged, washed several times with water, and dried. The product **M** was collected and re-dissolved in acetone-d_6 for NMR analysis. ^{1}H NMR (500 MHz, acetone-d_6) δ (ppm): 8.98 (d, J = 5.0 Hz, 4H), 8.11 (d, J = 10.0 Hz, 4H), 7.83 (d, J = 15.0 Hz, 4H), 7.70 (d, J = 10.0 Hz, 4H), 7.57 (d, J = 10.0 Hz, 4H), 7.30 (d, J = 10.0 Hz, 4H), 7.04 (d, J = 10.0 Hz, 4H), 6.78 (d, J = 10.0 Hz, 4H), 3.99 (t, J = 10.0 Hz, 4H), 2.50 (t, J = 10.0 Hz, 4H), 1.78–1.83 (m, 4H), 1.68–1.74 (m, 4H), 1.60–1.64 (m, 4H), 1.49–1.50 (m, 24H), 1.13–1.25 (m, 36H). ^{31}P NMR (202 MHz, acetone-d_6) δ (ppm): 14.22 ($J_{Pt\text{-}P}$ = 2654.3 Hz). ^{13}C NMR (126 MHz, acetone-d_6) δ (ppm): 159.22, 153.48, 150.71, 137.04, 134.07, 133.84, 133.43, 133.37, 130.05, 127.58, 125.18, 120.63, 114.69, 26.04, 25.94, 17.10, 13.27, 13.11, 12.94, 7.86. ESI-TOF-MS: Calculated for [**M** – 5PF_6^-]$^{5+}$: m/z = 1080.0123, [**M** – 4PF_6^-]$^{4+}$: m/z = 1386.2565, [**M** – 3PF_6^-]$^{3+}$: m/z = 1896.6636; Found: m/z = 1080.0124, m/z = 1386.2562.

Compounds **3** and **4** were synthesized according to the literatures[1-2].

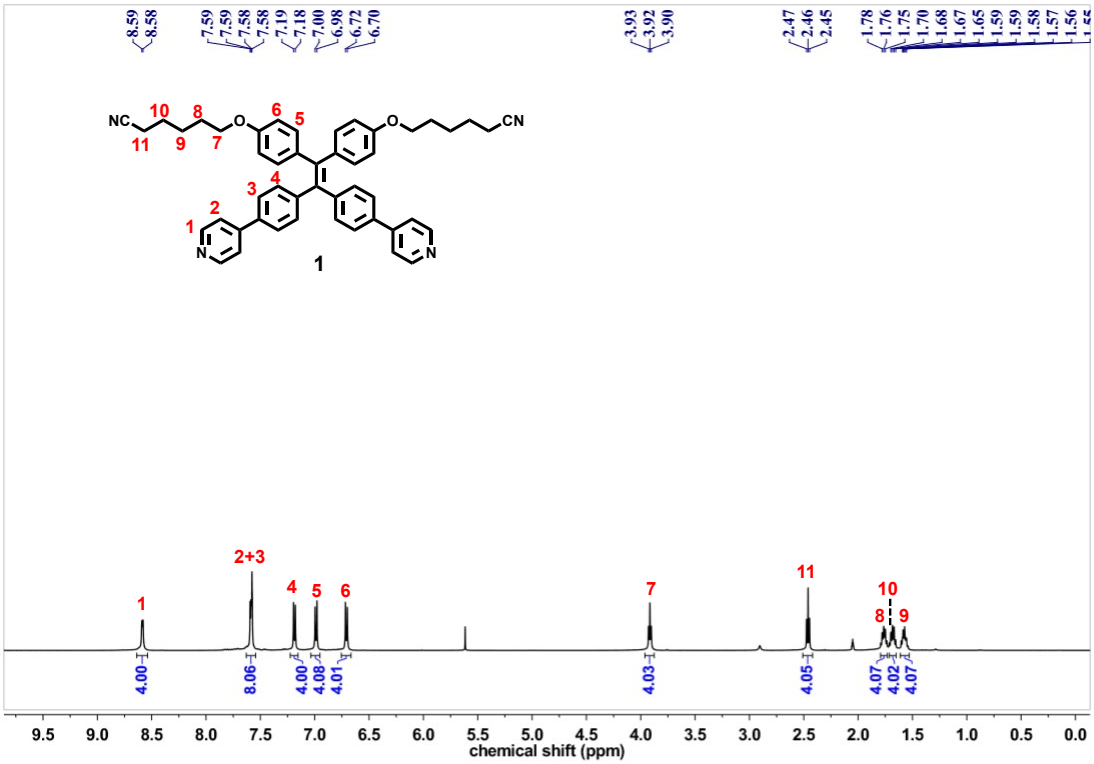

Figure S1. ^{1}H NMR (500 MHz, acetone-d_6, 298 K) spectrum of **1**.

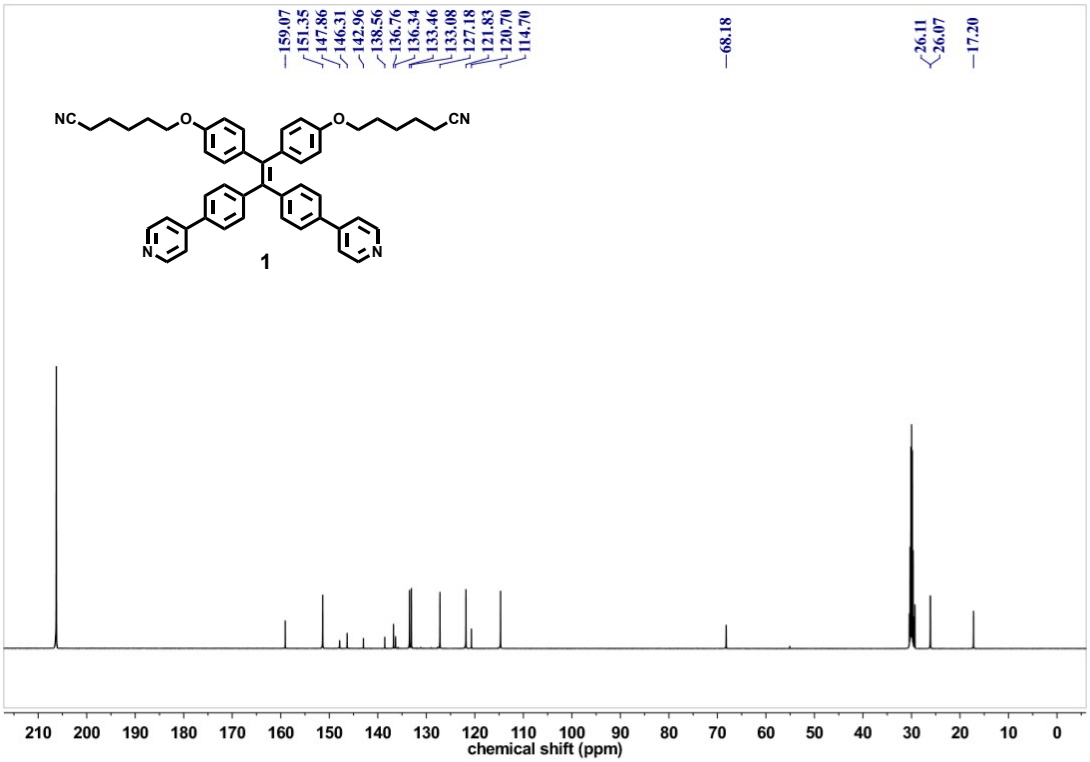

Figure S2. ^{13}C NMR (126 MHz, acetone-d_6, 298 K) spectrum of **1**.

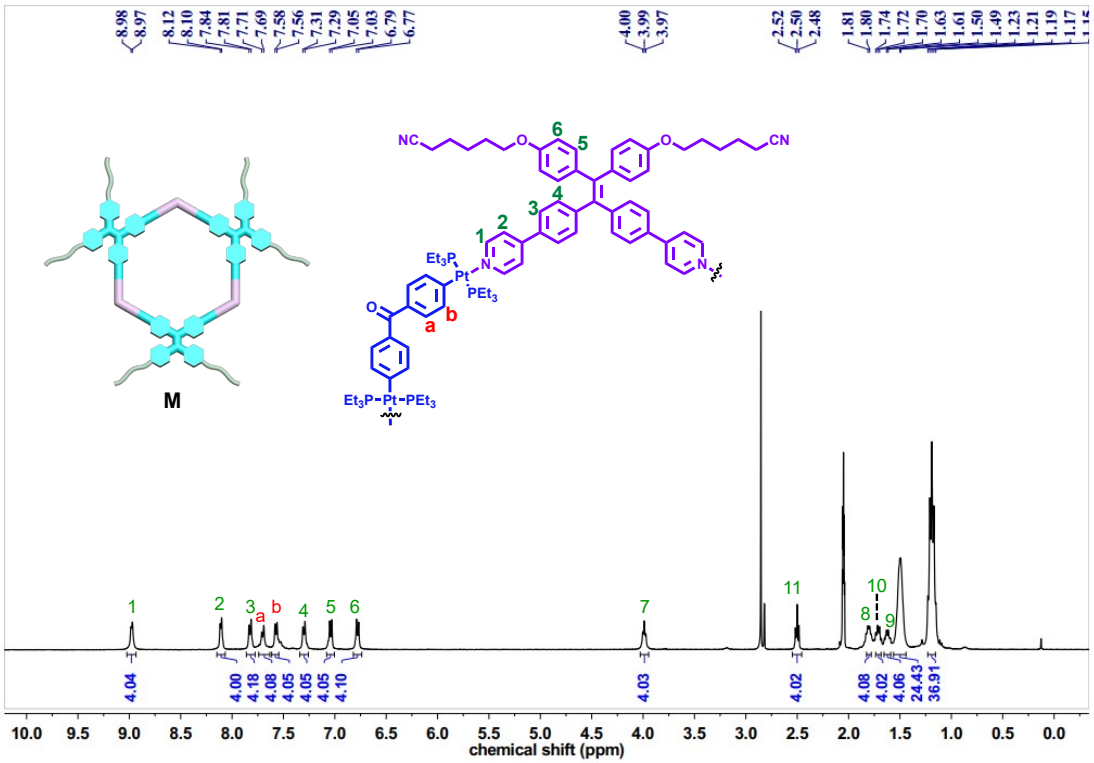

Figure S3. ^{1}H NMR (500 MHz, acetone-d_6, 298 K) spectrum of **M**.

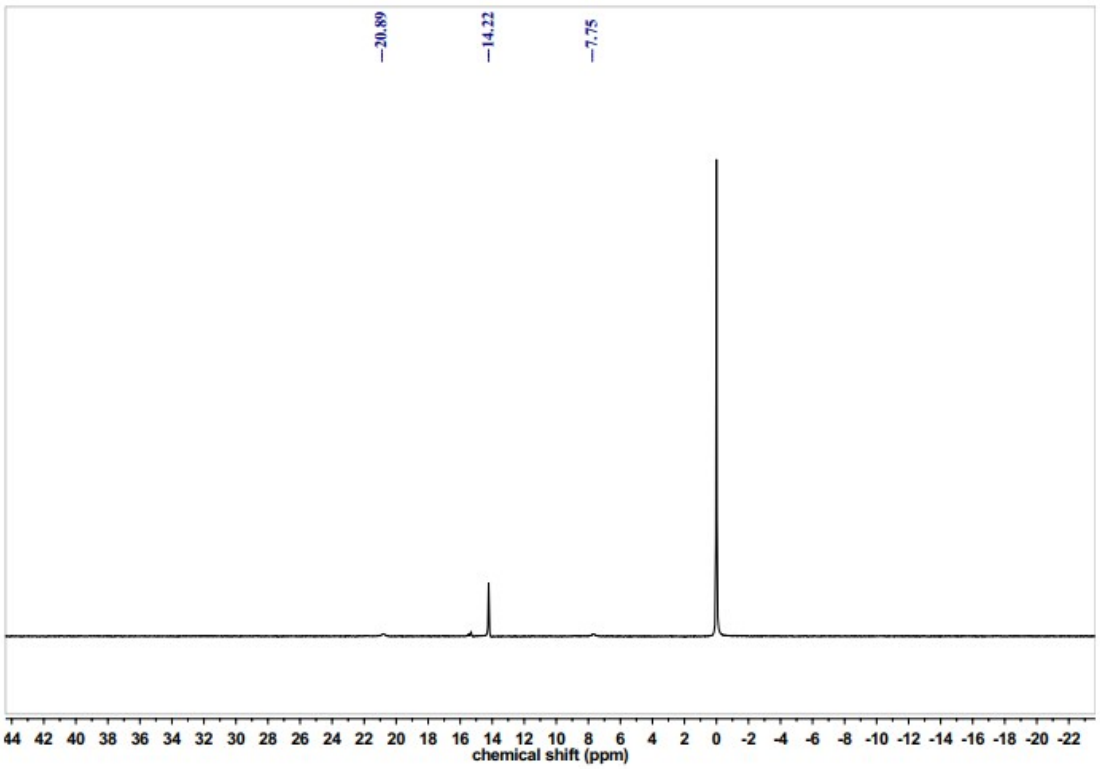

Figure S4. ^{31}P NMR (202 MHz, acetone-d_6, 298 K) spectrum of **M**.

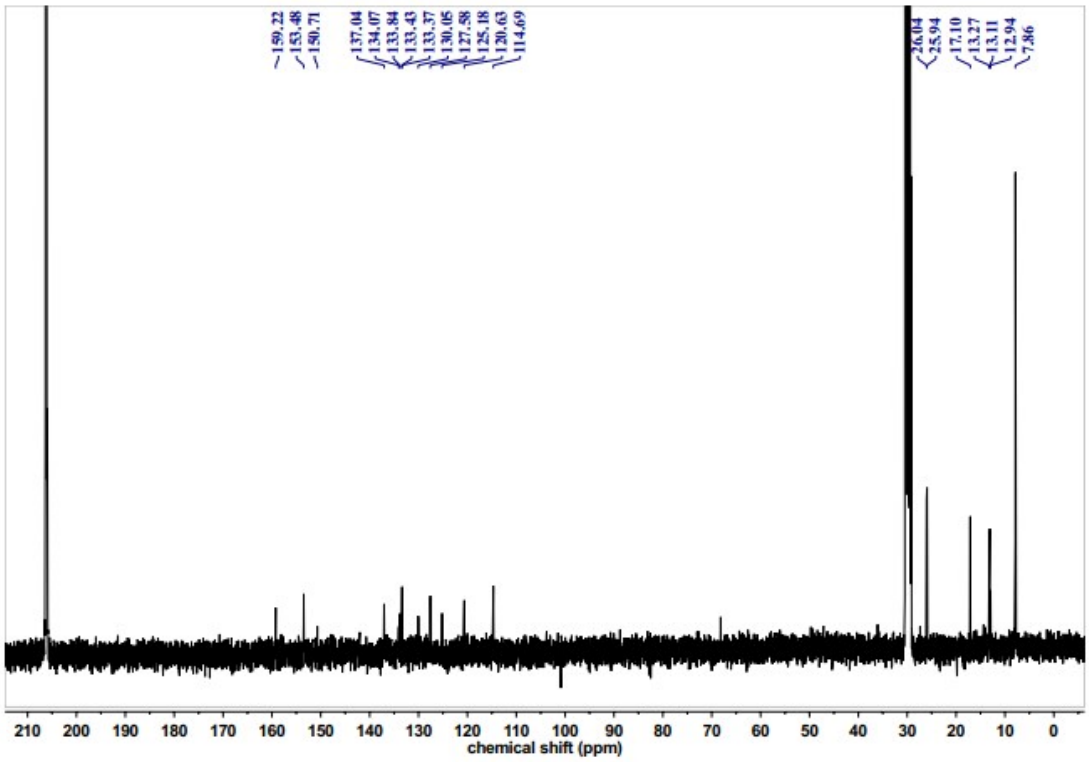

Figure S5. ^{13}C NMR (126 MHz, acetone-d_6, 298 K) spectrum of **M**.

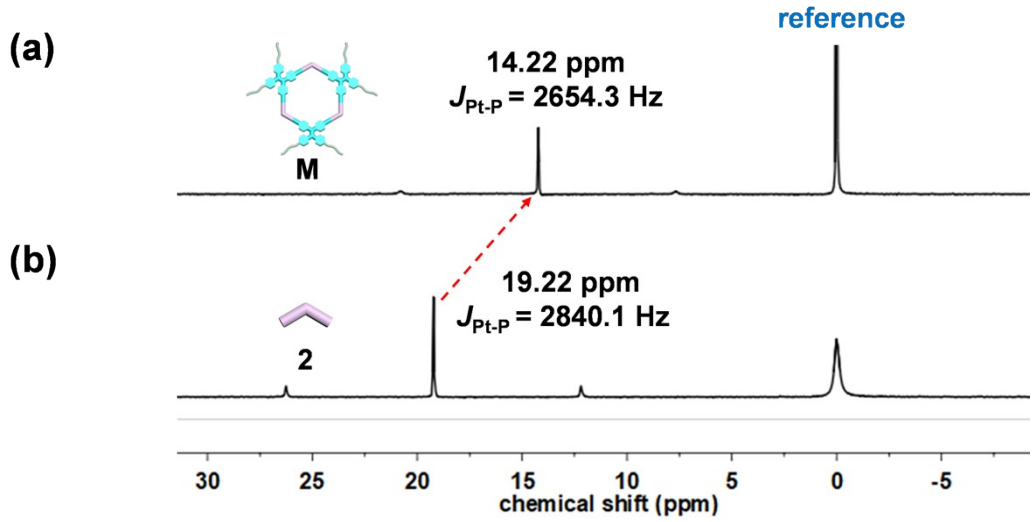

Figure S6. Partial ^{31}P {1H} NMR spectra (202 MHz, acetone-d_6, 298 K) of self-assembled hexagon metallacycle **M** (a) and 120° diplatinum(II) acceptor **2** (b).

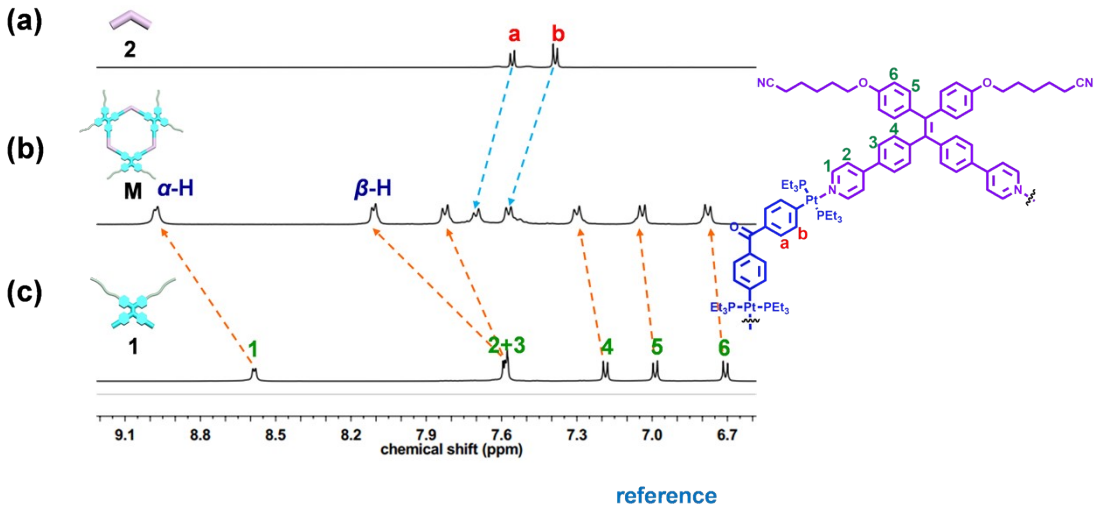

Figure S7. Partial ^{1}H NMR spectra (500 MHz, acetone-d_6, 298 K) of 120° diplatinum(II) acceptor **2** (a), self-assembled hexagon metallacycle **M** (b) and 120° dipyridyl donor **1** (c).

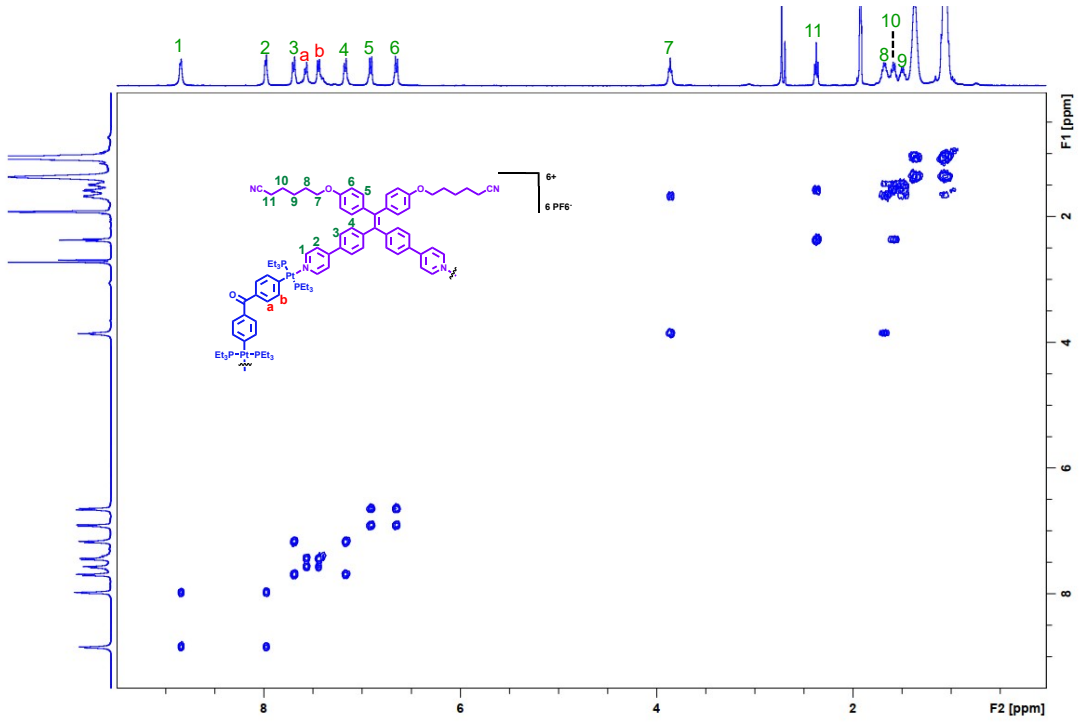

Figure S8. 2D COSY NMR (500 MHz, acetone-d_6, 298 K) spectrum of **M**.

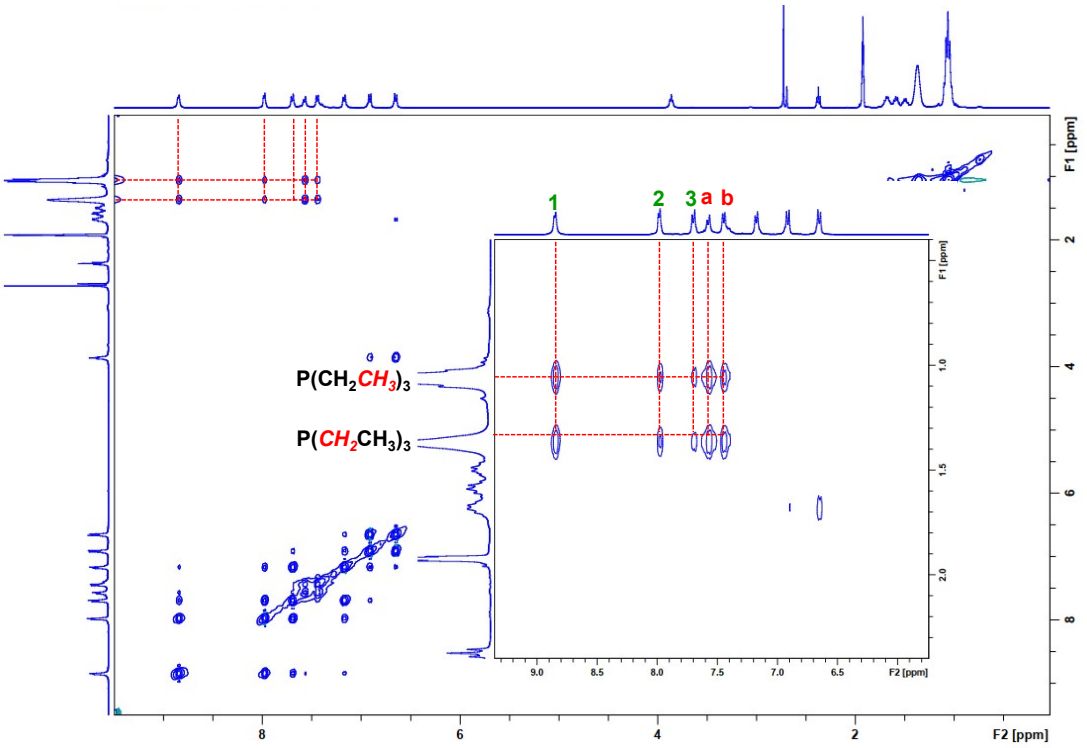

Figure S9. 2D NOESY NMR (400 MHz, acetone-d_6, 298 K) spectrum of **M**.

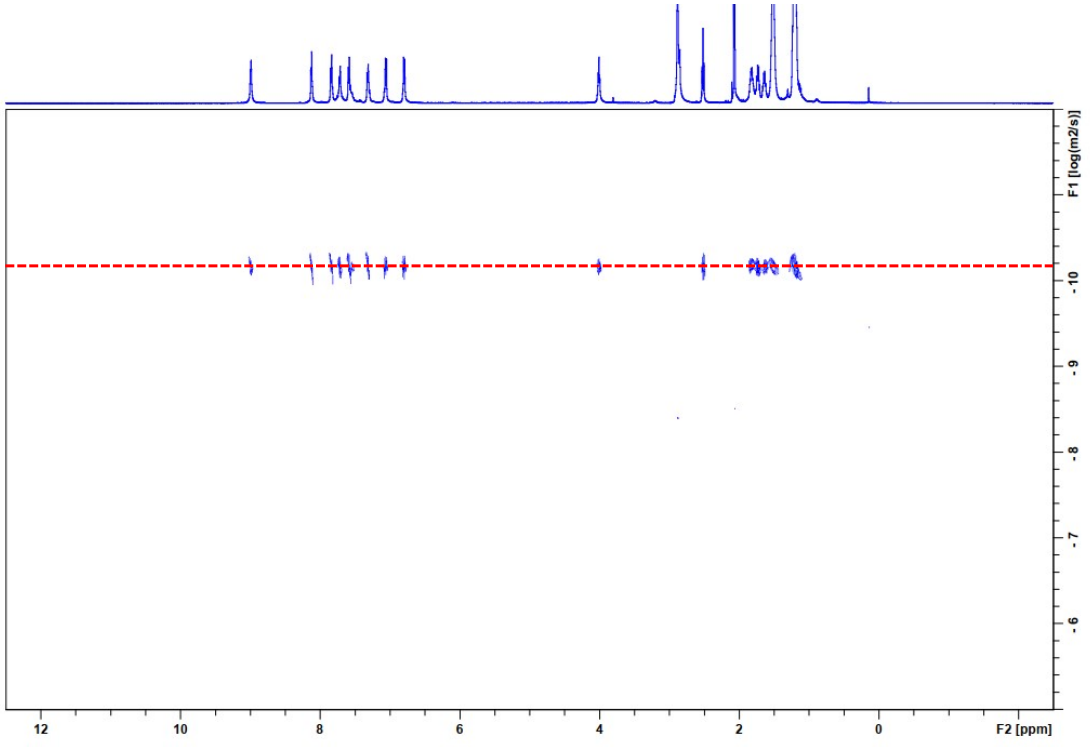

Figure S10. 2D DOSY NMR (500 MHz, acetone-d_6, 298 K) spectrum of **M**.

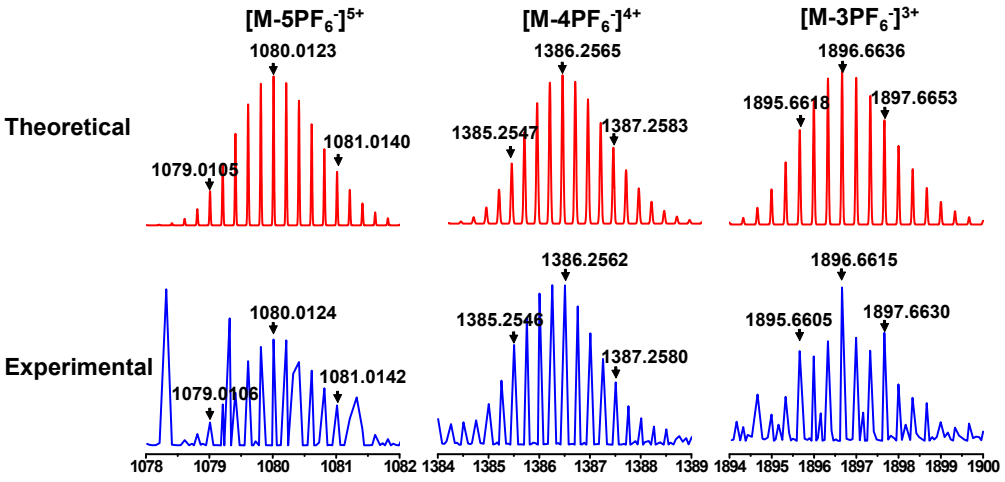

Figure S11. Theoretical (top) and experimental (bottom) ESI-TOF-MS of rhomboidal metallacycle **M**.

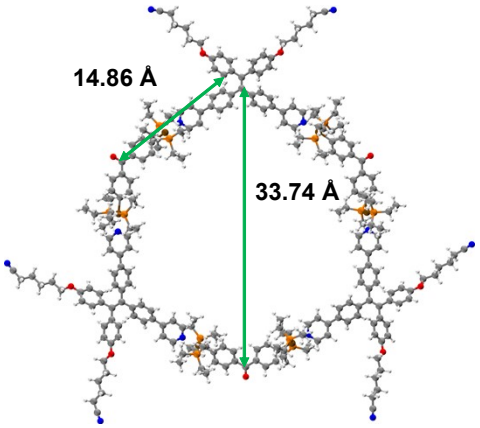

Figure S12. Simulation geometric structures of the self-assembled metallacycle **M** optimized by the GFN2-xTB semiempirical tight-binding method[3]

3. Host-guest complexation studies in dilute solution.

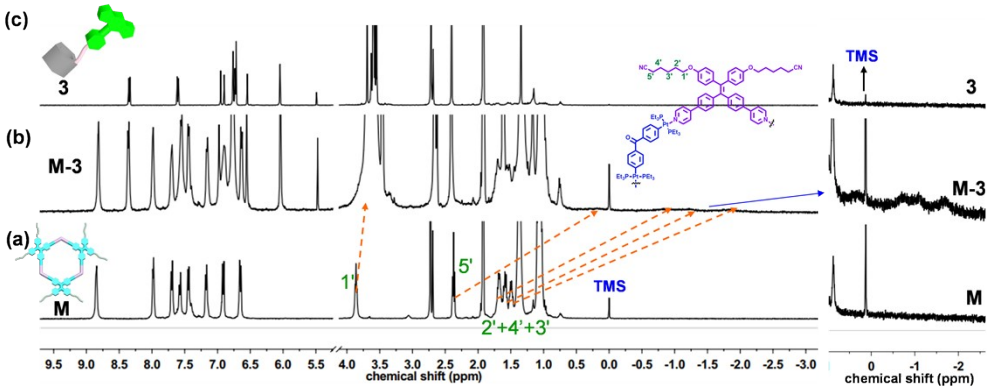

Figure S13. ^{1}H NMR spectra (500 MHz, acetone-d_6, 298 K) of 1.0 mM **M** (a), 1.0 mM **M** and 6.0 mM **3** (b), and 6.0 mM **3** (c).

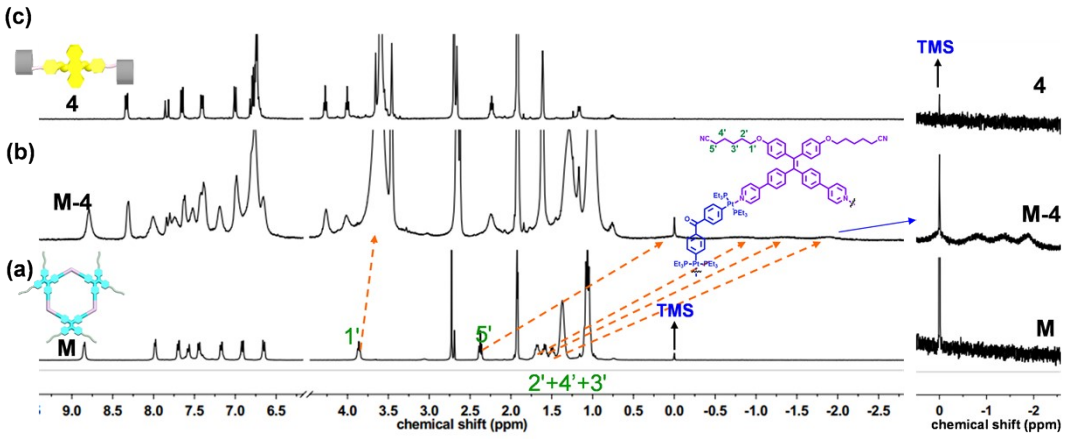

Figure S14. ^{1}H NMR spectra (500 MHz, acetone-d_6/THF-d_8(v/v, 4/1), 298 K) of 1.0 mM **M** (a), 1.0 mM **M** and 3.0 mM **4** (b), and 3.0 mM **4** (c).

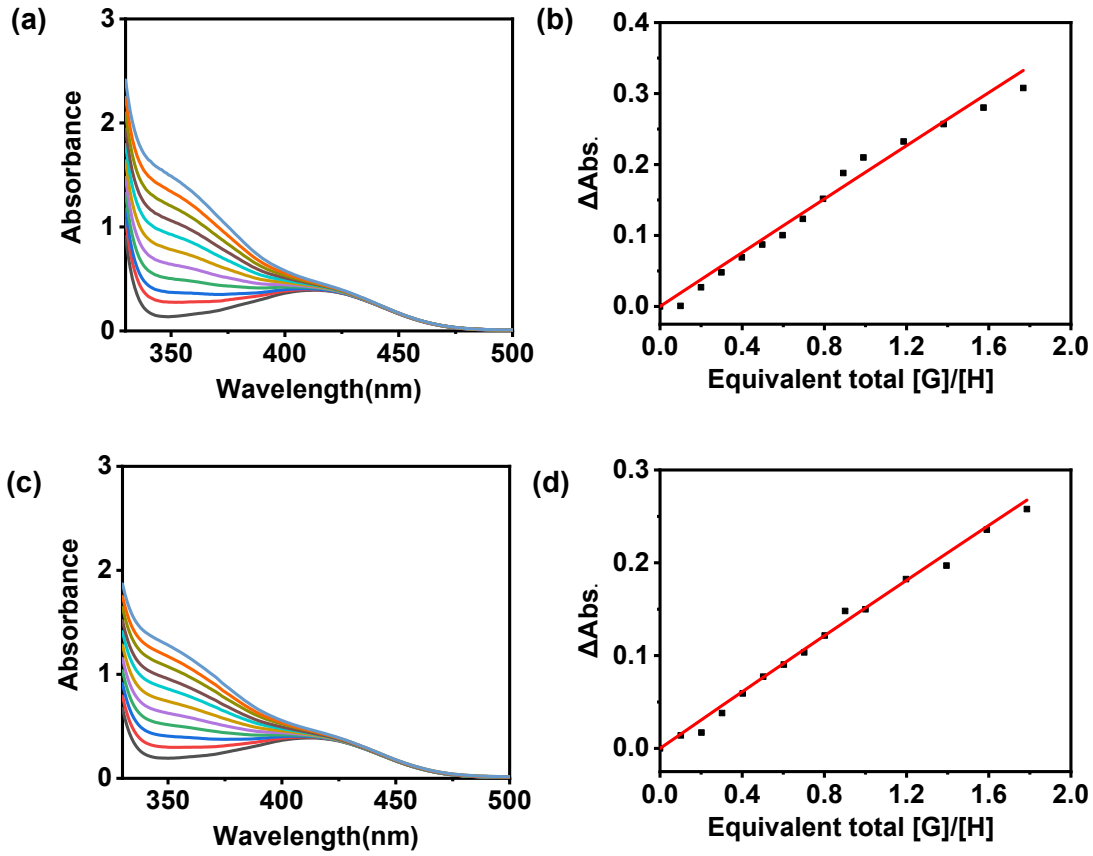

Figure S15. The UV/vis titration of pillar[5]arene ligand **4** with the addition of ligand **1** in acetone (a) and in acetone/water (v/v, 9/1) (c). By using the website (http://app.supramolecular.org/bindfit), the binding constant was calculated to be K = 389.08 ± 5.16 M^{-1} in acetone (b) and K = 676.15 ± 4.62 M^{-1} in acetone/water (v/v, 9/1) (d), respectively.

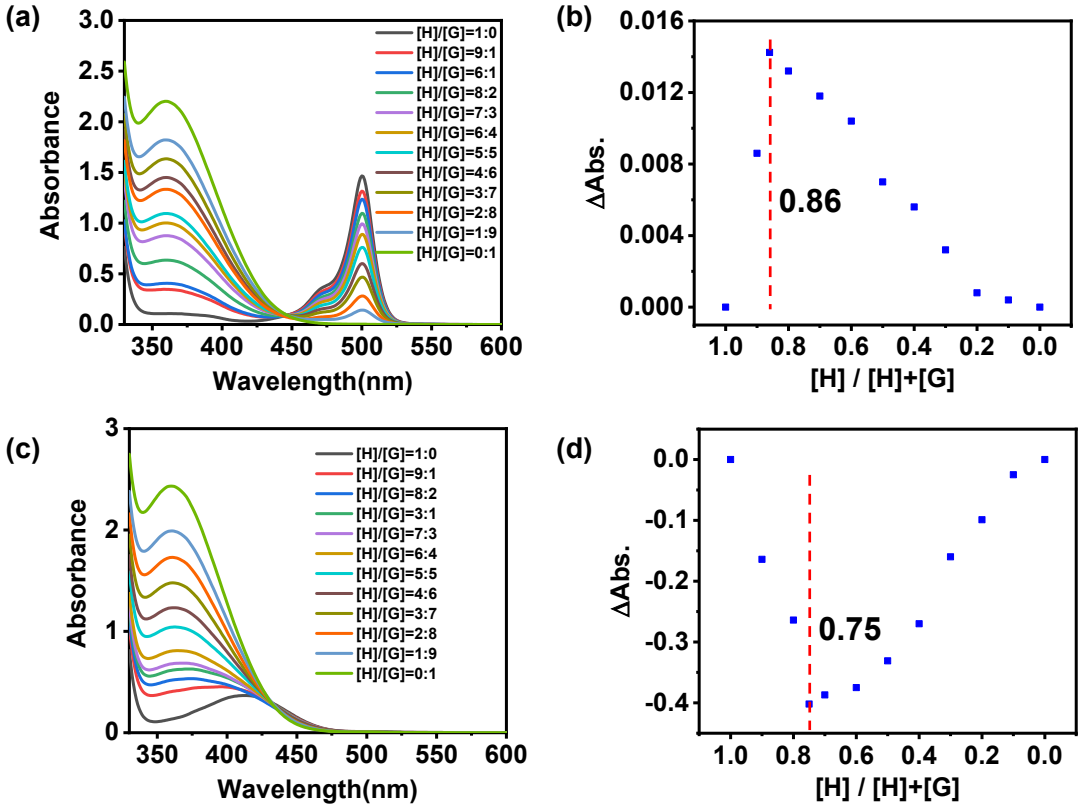

Figure S16. (a) The UV-vis spectra in acetone of pillar[5]arene ligand **3** (Host) with the addition of metallacycle **M** (Guest) ([**3**] + [**M**] = 20 μM). (b) Job plot for long-chain alkyl-CN-containing metallacycle **M** and pillar[5]arene ligand **3** in acetone ([**M**] + [**3**] = 20 μM). (c) The UV-vis spectra in acetone of pillar[5]arene ligand **4** (Host) with the addition of metallacycle **M** (Guest) ([**4**] + [**M**] = 20 μM). (d) Job plot for long-chain alkyl-CN-containing metallacycle **M** and pillar[5]arene ligand **4** in acetone ([**M**] + [**4**] = 20 μM).

4. Photophysical properties study

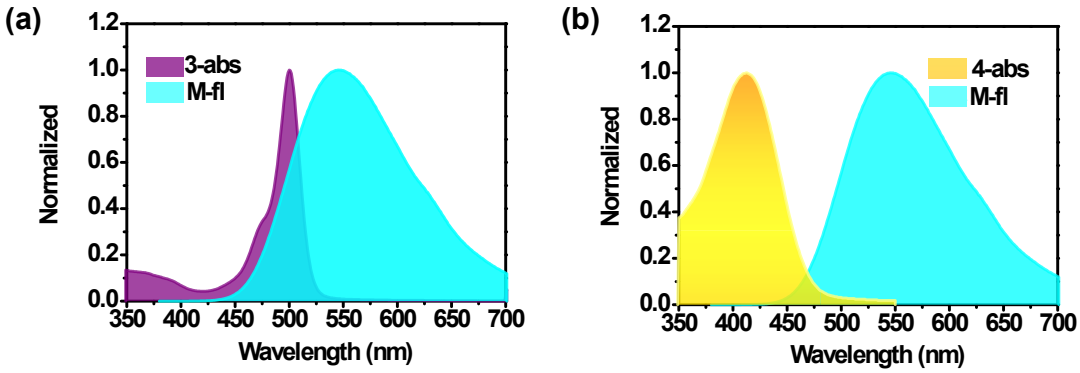

Figure S17. (a) Normalized emission spectrum of **M** and absorption spectrum of **3**. (b) Normalized emission spectrum of **M** and absorption spectrum of **4**.

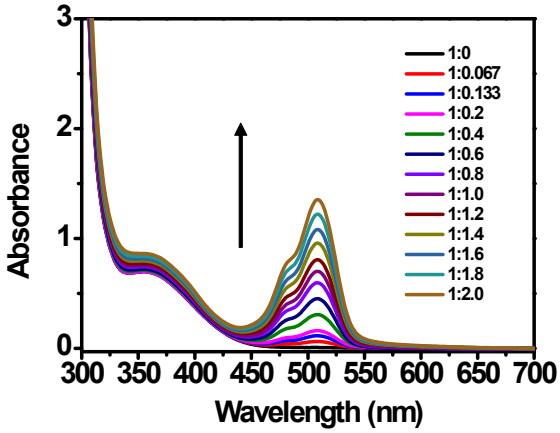

Figure S18. Absorption spectra of **M** with the addition of **3** in the acetone/water (1/9, v/v) ([TPE unit] = 20 μM).

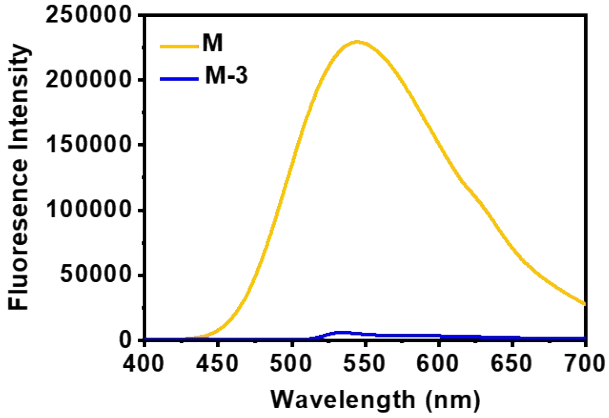

Figure 19. Fluorescence emission spectra of **M** and **M-3** in the acetone/water mixtures (1/9) (λ_{ex} = 365 nm, slit (5, 5), [TPE unit] = 20 μM, [BODIPY unit] = 40 μM)

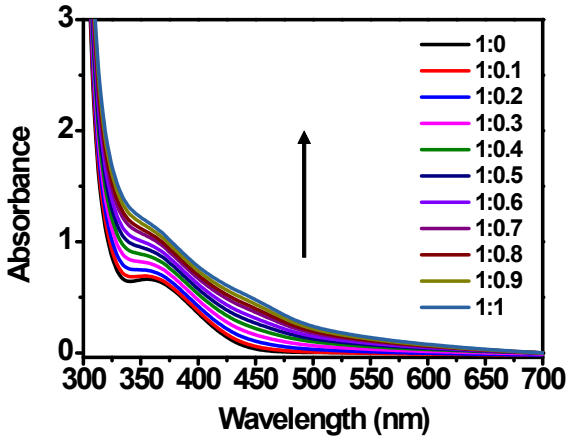

Figure S20. Absorption spectra of **M** with the addition of **4** in the acetone/water (1/9, v/v) ([TPE unit] = 20 μM).

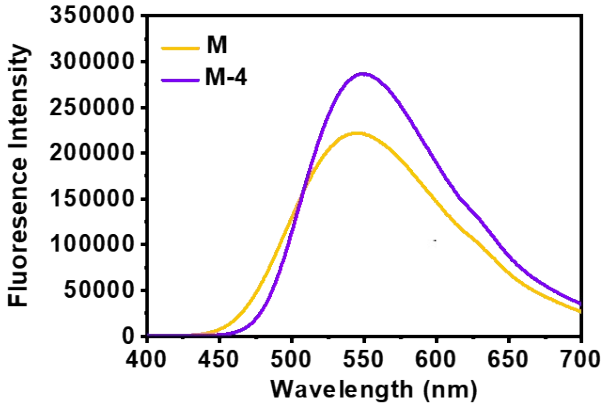

Figure S21. Fluorescence emission spectra of **M** and **M-4** in the acetone/water mixtures (1/9, v/v) (λ_{ex} = 365 nm, slit (5, 5), [TPE unit] = 20 μM, [DSA unit] = 20 μM).

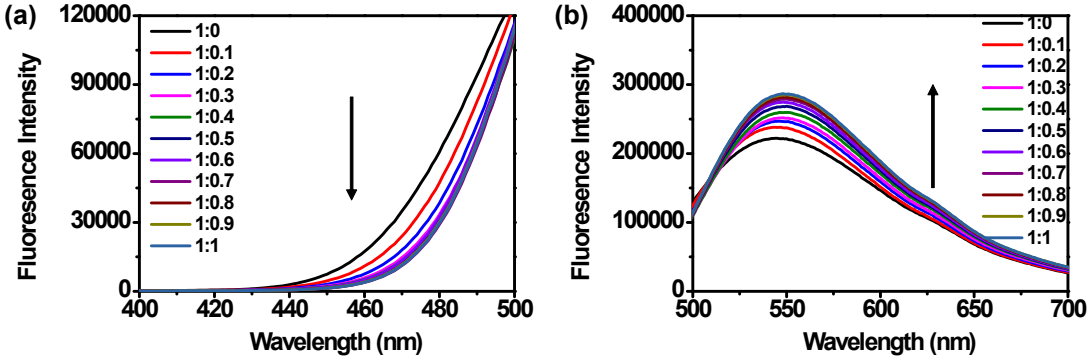

Figure S22. Fluorescence emission spectra at 400-500 nm (a) and at 500-700 nm (b) of **M** with the addition of **4** in the acetone/water (1/9, v/v) (λ_{ex} = 365 nm, [TPE unit] = 20 μM).

Table S1. The fluorescence lifetime of **M-3-5** in the mixtures of acetone/water (1/9, v/v).

	τ_1/ns	RW_1[%]	τ_2/ns	RW_2[%]	τ
M	1.41	98.5	4.49	1.5	1.55
M-3 (1:6)	0.95	100	---	---	0.95
M-3-5 (1:6:0.067)	0.81	100	---	---	0.82

Table S2. The fluorescence lifetime of **M-4-5** in the mixtures of acetone/water (1/9, v/v).

	τ_1/ns	RW_1[%]	τ_2/ns	RW_2[%]	τ
M	1.41	98.5	4.49	1.5	1.55
M-4 (1:3)	1.21	99.2	4.17	0.8	1.28
M-4-5 (1:3:0.100)	1.13	99.8	5.09	0.2	1.17

5. Morphology characterization

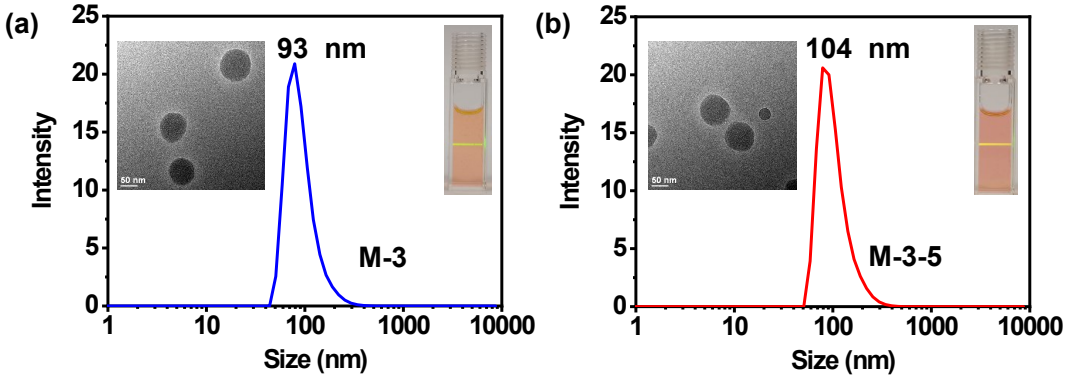

Figure S23. DLS data and TEM image of **M-3** (a), **M-3-5** (b) in the acetone/water (1/9, v/v) ([TPE unit] = 20 μM, [BODIPY unit] = 40 μM, [NiR unit] = 0.447 μM). Inset: Photograph of the Tyndall effect.

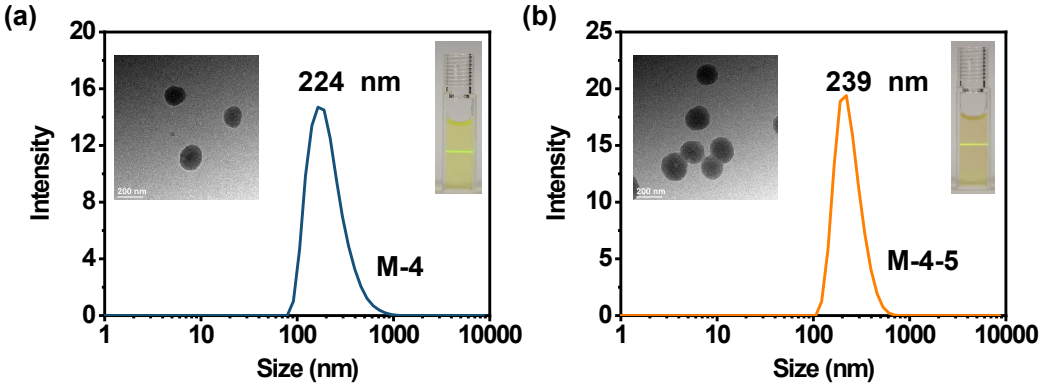

Figure S24. DLS data and TEM image of **M-4** (a), **M-4-5** (b) in the acetone/water (1/9, v/v) ([TPE unit] = 20 μM, [DSA unit] = 20 μM, [NiR unit] = 0.667 μM). Inset: Photograph of the Tyndall effect.

6. Calculations of energy transfer efficiency and antenna effect

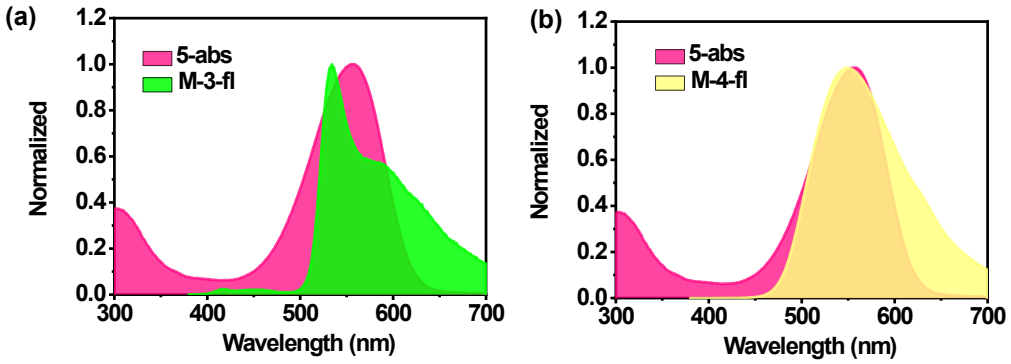

Figure S25. (a) Normalized emission spectrum of **M-3** and absorption spectrum of **5**. (b) Normalized emission spectrum of **M-4** and absorption spectrum of **5**.

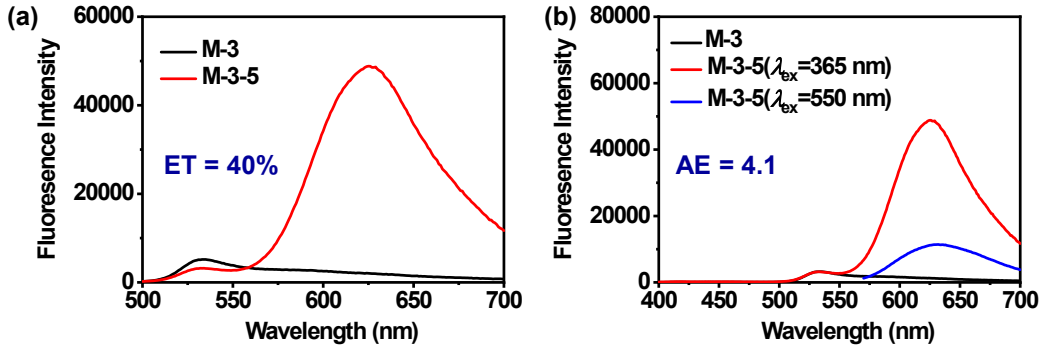

Figure S26. (a) Fluorescence emission spectra of **M-3** (1:6) and **M-3-5** (1:6:0.067) in acetone/water. (b) Fluorescence emission spectra of **M-3** (1:6) (black line normalized according to the intensity at 530 nm of the red line), **M-3-5** (1:6:0.067) at 365 nm (red line) and 550 nm (blue line) in the acetone/water (1/9, v/v) (slit (5 nm, 5 nm), [TPE unit] = 20 μM, [BODIPY unit] = 40 μM, [NiR unit] = 0.447 μM).

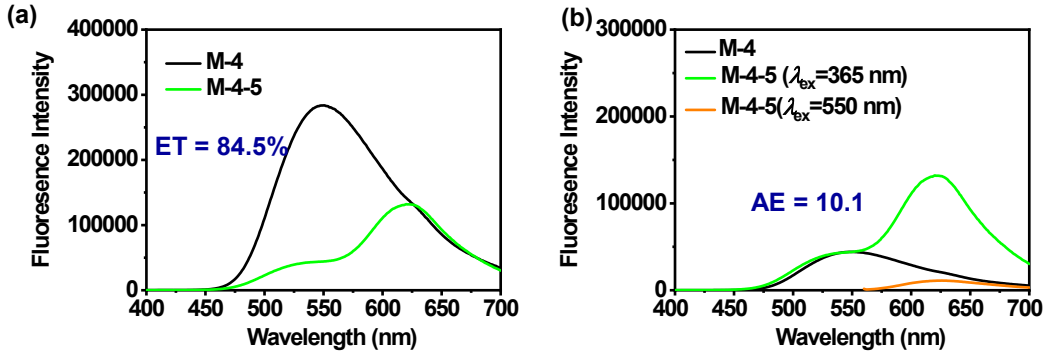

Figure S27. (a) Fluorescence emission spectra of **M-4** (1:3) and **M-4-5** (1:3:0.1) in acetone/water. (b) Fluorescence emission spectra of **M-4** (1:3) (black line normalized according to the intensity at 530 nm of the green line), **M-4-5** (1:3:0.1) at 365 nm (green line) and 550 nm (orange line) in acetone/water (1/9, v/v) (slit (5 nm, 5 nm), [TPE unit] = 20 μM, [DSA unit] = 40 μM, [NiR unit] = 0.667 μM).

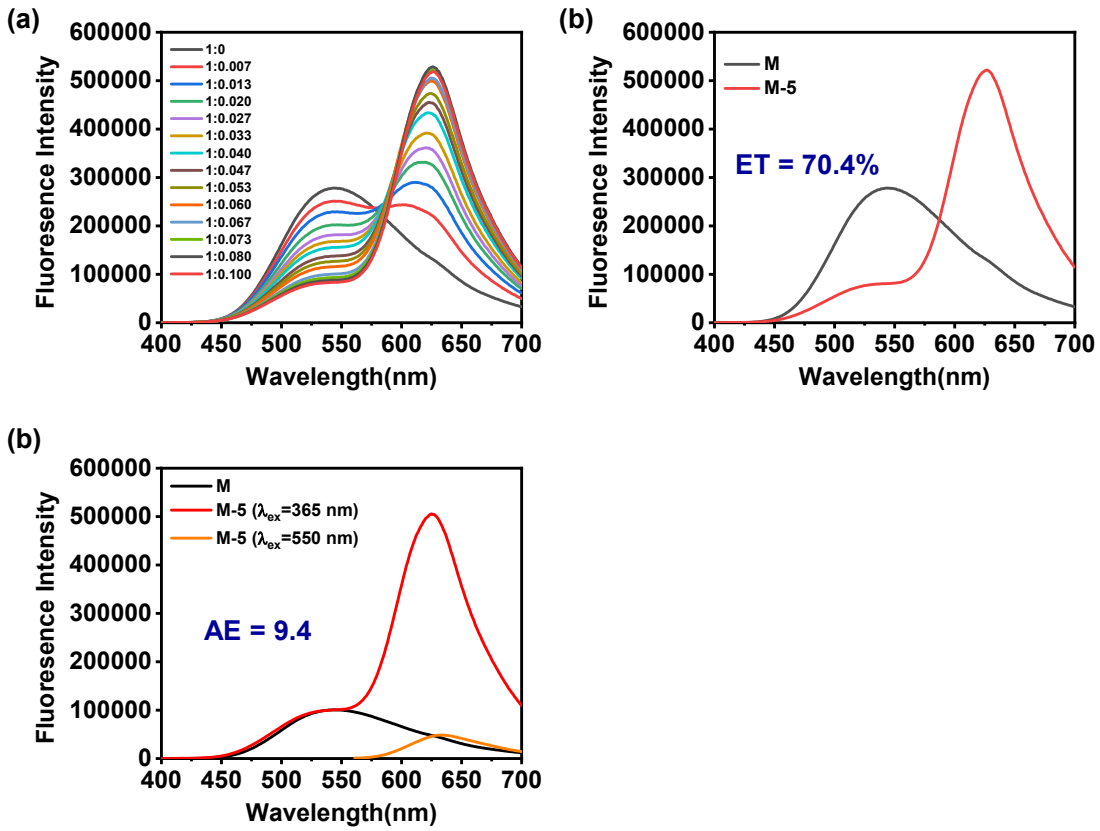

Figure S28. (a) Fluorescence emission spectra of **M** in acetone/water (1/9, v/v) with the addition of **5**. (b) Fluorescence emission spectra of **M-5** (1:0.1) in acetone/water. (c) Fluorescence emission spectra of **M** (back line normalized according to the intensity at 550 nm of the red line), **M-5** (1:0.1) at 365 nm (red line) and 550 nm (orange line) in acetone/water (1/9, v/v) (slit (5 nm, 5 nm), [TPE unit] = 20 μM, [NiR unit] = 0.667 μM).

7. DFT calculations

The structural optimization and molecular orbital calculations of TPE, BODIPY, DSA, and NiR are based on Gaussian16[4]. The optimization geometry task uses Becke's three-parameter hybrid functional with the Lee–Yang–Parr correlation functional (B3LYP)[5] and 6-31+G* basis set. Rendering of molecular orbitals and intermolecular interactions using IQmol software. Dispersion correction is performed using the Grimme-D3 (BJ) method[6].

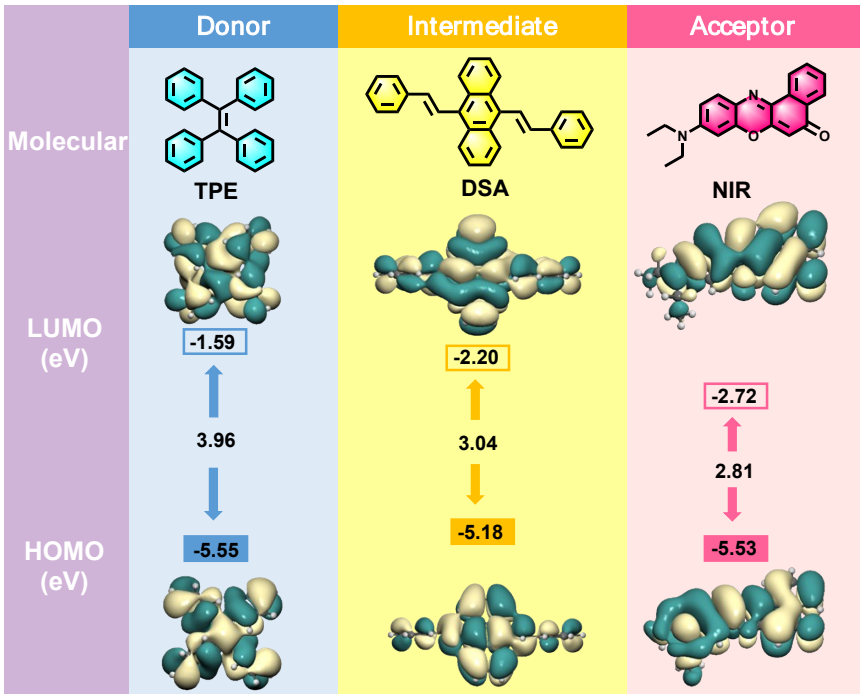

Figure S29. Calculated HOMO and LUMO orbitals and corresponding orbital energies of TPE, DSA, and NiR molecules.

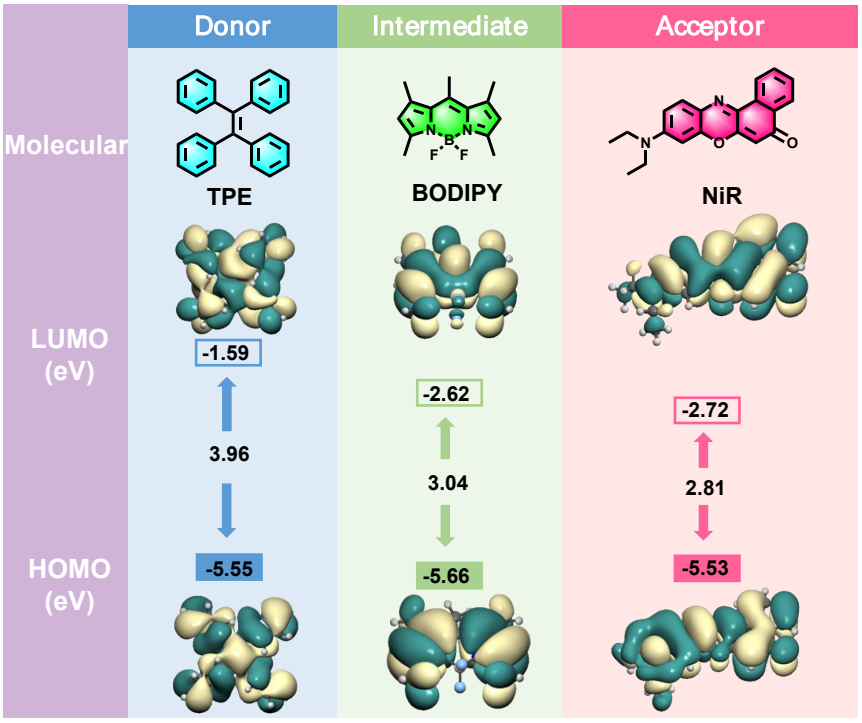

Figure S30. Calculated HOMO and LUMO orbitals and corresponding orbital energies of TPE, BODIPY, and NiR molecules.

8. References

[1] P.-P. Jia, L. Xu, Y.-X. Hu, W.-J. Li, X.-Q. Wang, Q.-H. Ling, X. Shi, G.-Q. Yin,

X. Li, H. Sun, Y. Jiang, H.-B. Yang, *J. Am. Chem. Soc.* **2021**, *143*, 399.

[2] G.-Y. Wu, X.-Q. Wang, L.-J. Chen, Y.-X. Hu, G.-Q. Yin, L. Xu, B. Jiang, H.-B. Yang, *Inorg. Chem.* **2018**, *57*, 15414.

[3] a) C. Bannwarth, S. Ehlert, S. Grimme, *J. Chem. Theory Comput.* **2019**, *15*, 1652. b) M. Bursch, H. Neugebauer, S. Grimme, *Angew. Chem. Int. Ed.* **2019**, *58*, 11078. c) W. Humphrey, A. Dalke, K. Schulten, *J. Mol. Graphics* **1996**, *14*, 33. d) Lu T, Chen F, *J. Comput. Chem.* **2012**, *33*, 580.

[4] M. J. Frisch, G. W. Trucks, H. B. Schlegel, G. E. Scuseria, M. A. Robb, J. R. Cheeseman, G. Scalmani, V. Barone, G. A. Petersson, H. Nakatsuji, X. Li, M. Caricato, A. V. Marenich, J. Bloino, B. G. Janesko, R. Gomperts, B. Mennucci, H. P. Hratchian, J. V. Ortiz, A. F. Izmaylov, J. L. Sonnenberg, D. Williams-Young, F. Ding, F. Lipparini, F. Egidi, J. Goings, B. Peng, A. Petrone, T. Henderson, D. Ranasinghe, V. G. Zakrzewski, J. Gao, N. Rega, G. Zheng, W. Liang, M. Hada, M. Ehara, K. Toyota, R. Fukuda, J. Hasegawa, M. Ishida, T. Nakajima, Y. Honda, O. Kitao, H. Nakai, T. Vreven, K. Throssell, J. A. Montgomery, Jr., J. E. Peralta, F. Ogliaro, M. J. Bearpark, J. J. Heyd, E. N. Brothers, K. N. Kudin, V. N. Staroverov, T. A. Keith, R. Kobayashi, J. Normand, K. Raghavachari, A. P. Rendell, J. C. Burant, S. S. Iyengar, J. Tomasi, M. Cossi, J. M. Millam, M. Klene, C. Adamo, R. Cammi, J. W. Ochterski, R. L. Martin, K. Morokuma, O. Farkas, J. B. Foresman, and D. J. Fox, Gaussian 16, Revision A.03, Gaussian, Inc., Wallingford CT, 2016.

[5] F. Weigend, R. Ahlrichs, *Phys. Chem. Chem. Phys.* **2005**, *7*, 3297.

[6] a) S. Grimme, J. Antony, S. Ehrlich, H. Krieg, *J. Chem. Phys.* **2010**, *132*, 154104; b) S. Grimme, S. Ehrlich, L. Goerigk, *J. Compt. Chem.* **2011**, *32*, 1456.